Biomedical Optics EXPRESS

Extraction of intrinsic fluorescence from single fiber fluorescence measurements on a turbid medium: experimental validation

U. A. Gamm,[1] C. L. Hoy,[1] F. van Leeuwen - van Zaane,[1] H. J. C. M. Sterenborg,[1] S. C. Kanick,[2] D. J. Robinson,[3] and A. Amelink[1,*]

[1] *Center for Optical Diagnostics and Therapy, Department of Radiation Oncology, Postgraduate school Molecular Medicine, Erasmus Medical Center, PO Box 2040, 3000 CA Rotterdam, The Netherlands*

[2] *Thayer School of Engineering, Dartmouth College, 8000 Cummings Hall, Hanover, New Hampshire 03755, USA*

[3] *Department of Otorhinolaryngology-Head and Neck Surgery, Erasmus Medical Center, PO Box 2040, 3000 CA Rotterdam, The Netherlands*

*arjen.amelink@tno.nl

Abstract: The detailed mechanisms associated with the influence of scattering and absorption properties on the fluorescence intensity sampled by a single optical fiber have recently been elucidated based on Monte Carlo simulated data. Here we develop an experimental single fiber fluorescence (SFF) spectroscopy setup and validate the Monte Carlo data and semi-empirical model equation that describes the SFF signal as a function of scattering. We present a calibration procedure that corrects the SFF signal for all system-related, wavelength dependent transmission efficiencies to yield an absolute value of intrinsic fluorescence. The validity of the Monte Carlo data and semi-empirical model is demonstrated using a set of fluorescent phantoms with varying concentrations of Intralipid to vary the scattering properties, yielding a wide range of reduced scattering coefficients (μ_s' = 0-7 mm^{-1}). We also introduce a small modification to the model to account for the case of μ_s' = 0 mm^{-1} and show its relation to the experimental, simulated and theoretically calculated value of SFF intensity in the absence of scattering. Finally, we show that our method is also accurate in the presence of absorbers by performing measurements on phantoms containing red blood cells and correcting for their absorption properties.

© 2014 Optical Society of America

OCIS codes: (060.2310) Fiber optics and optical communications; (170.6280) Spectroscopy, fluorescence and luminescence.

References and links

1. J. Quincy Brown, K. Vishwanath, G. M. Palmer, and N. Ramanujam, "Advances in quantitative UV-visible spectroscopy for clinical and pre-clinical application in cancer," Curr. Opin. Biotechnol. **20**, 119–131 (2009).
2. C. Mujat, C. Greiner, A. Baldwin, J. M. Levitt, F. Tian, L. A. Stucenski, M. Hunter, Y. L. Kim, V. Backman, M. Feld, K. Münger, and I. Georgakoudi, "Endogenous optical biomarkers of normal and human papillomavirus immortalized epithelial cells," Int. J. Cancer **122**, 363–371 (2008).

#203123 - $15.00 USD Received 17 Dec 2013; revised 9 Feb 2014; accepted 10 Feb 2014; published 22 May 2014

3. M. C. Skala, G. M. Palmer, C. Zhu, Q. Liu, K. M. Vrotsos, C. L. Marshek-Stone,A. Gendron-Fitzpatrick, and N. Ramanujam, "Investigation of fiber-optic probe designs for optical spectroscopic diagnosis of epithelial precancers," Laser Surg. Med. **34**, 25–38 (2004).
4. D. J Robinson, M. B. Karakullukcu, B. Kruijt, S. C. Kanick, R. P. L. van Veen, A. Amelink, H. J. C. M. Sterenborg, M. J. H. Witjes, and I. B. Tan, "Optical Spectroscopy to Guide Photodynamic Therapy of Head and Neck Tumors," IEEE J. Sel. Top. Quantum Electron. **16**, 854–862 (2010).
5. B. Karakullukcu, S. C. Kanick, J. B. Aans, H. J. C. M. Sterenborg, I. B. Tan, A. Amelink, and D. J. Robinson, "Clinical feasibility of monitoring m-THPC mediated photodynamic therapy by means of fluorescence differential path-length spectroscopy," J. Biophotonics **4**, 740–751 (2011).
6. T. M. Baran, and T. H. Foster, "Recovery of Intrinsic Fluorescence From Single-Point Interstitial Measurements for Quantification of Doxorubicin Concentration," Laser Surg. Med. **45**, 542–550 (2013).
7. J. Wu, M. S. Feld, and R. P Rava, "Analytical model for extracting intrinsic fluorescence in turbid media," Appl. Opt. **19**, 3585–3595 (1993).
8. C. M. Gardner, S. L. Jacques, and A. J. Welch, "Fluorescence spectroscopy of tissue: recovery of intrinsic fluorescence from measured fluorescence," Appl. Opt. **35**, 1780–1792 (1996).
9. M. G. Mller, I. Georgakoudi, Q. Zhang, J. Wu, and M. S. Feld, "Intrinsic fluorescence spectroscopy in turbid media: disentangling effects of scattering and absorption," Appl. Opt. **40**, 4633–4646 (2001).
10. Q. Zhang, M. G. Mller, J. Wu, and M. S. Feld, "Turbidity-free fluorescence spectroscopy of biological tissue," Opt. Lett. **25**, 1451–1453 (2000).
11. J. C. Finlay and T. H. Foster, "Recovery of hemoglobin oxygen saturation and intrinsic fluorescence with a forward-adjoint model," Appl. Opt. **44**, 1917–1933 (2005).
12. G. M. Palmer and N. Ramanujam, "Monte-carlo-based model for the extraction of intrinsic fluorescence from turbid media," J. Biomed. Opt. **13**, 024017 (2008).
13. G. M. Palmer. R. J. Viola, T. Schroeder, P. S. Yarmolenko, M. W. Dewhirst, and N. Ramanujam, "Quantitative diffuse reflectance and fluorescence spectroscopy: tool to monitor tumor physiology in vivo," J. Biomed. Opt. **14**, 024010 (2009).
14. R. H. Wilson, M. Chandra, J. Scheiman, D. Simeone, B. McKenna, J. Purdy, and M. A. Mycek, "Optical spectroscopy detects histological hallmarks of pancreatic cancer," Opt. Express **17**, 17502–17516 (2009).
15. A. Kim, M. Khurana, Y. Moriyama, and B. C. Wilson, "Quantification of in vivo fluorescence decoupled from the effects of tissue optical properties using fiber-optic spectroscopy measurements," J. Biomed. Opt. **15**, 067006 (2010).
16. J. C. Finlay, T. C. Zhu, A. Dimofte, D. Stripp, S. B. Malkowicz, T. M. Busch, and S. M. Hahn, "Interstitial fluorescence spectroscopy in the human prostate during motexafin lutetium-mediated photodynamic therapy," Photochem. Photobiol. **82**, 1270–1278 (2006).
17. B. W. Pogue and G. Burke, "Fiber-optic bundle design for quantitative fluorescence measurement from tissue", Appl. Opt. **37**, 7429–7436 (1998).
18. T. J. Pfefer, K. T. Schomacker, M. N. Ediger, and N. S. Nishioka, "Light propagation in tissue during fluorescence spectroscopy with single-fiber probes," IEEE J. Sel. Top. Quantum Electron. **7**, 1004–1012 (2001).
19. K. R. Diamond, M. S. Patterson, and T. J. Farrell, "Quantification of fluorophore concentration in tissue-simulating media by fluorescence measurements with a single optical fiber," Appl. Opt. **42**, 2436–2442 (2003).
20. H. Stepp, T. Beck, W. Beyer, C. Pfaller, M. Schuppler, R. Sroka, and R. Baumgartner, "Measurement of fluorophore concentration in turbid media by a single optical fiber," Medical Laser Application **22**, 23–34 (2007).
21. S. C. Kanick,. D. J. Robinson, H. J. C. M. Sterenborg, and A. Amelink, "Semi-empirical model of the effect of scattering on single fiber fluorescence intensity measured on a turbid medium," Biomed. Opt. Express **3**, 137–152 (2012).
22. S. C. Kanick,. D. J. Robinson, H. J. C. M. Sterenborg, and A. Amelink, "Extraction of intrinsic fluorescence from single fiber fluorescence measurements on a turbid medium," Opt. Lett. **37**, 948–950 (2012).
23. M. C. Hudson, "Calculation of the maximum optical coupling efficiency into multimode optical waveguides," Appl. Opt. **13**, 1029–1033 (1974).
24. W. H. Park, "Fluorescence lifetime sensor using optical fiber and optical signal processing," thesis, University of Toronto (1998).
25. R. Michels, F. Foschum, and A. Kienle, "Optical properties of fat emulsions," Opt. Express **16**, 5907–5925 (2008).
26. R. Sjoback, J. Nygren, and M. Kubista, "Absorption and fluorescence properties of fluorescein," Spectrochim. Acta A **51**, L7-L21 (1995).
27. S. C. Kanick, D. J. Robinson, H. J. C. M. Sterenborg,A. Amelink, "Method to quantitate absorption coefficients from single fiber reflectance spectra without knowledge of the scattering properties.," Opt. Lett. **36**, 2791–2793 (1995).
28. N. Barbero, E. Barni, C. Barolo, P. Quagliotto, G. Viscardi, L. Napione, S. Pavan, F. Fussolino, "A study of the interaction between fluorescein sodium salt and bovine serum albumin by steady-state fluorescence," Dyes Pigm. **3**, 302–313 (2009).
29. E. Evans, D. Berk, A. Leung, "Detachment of agglutinin-bonded red blood cells. I. Forces to rupture molecular-

#203123 - $15.00 USD Received 17 Dec 2013; revised 9 Feb 2014; accepted 10 Feb 2014; published 22 May 2014
(C) 2014 OSA

point attachments," Biophys. J. **59**, 838–848 (2001).
30. S. C. Kanick, U. A.Gamm, H .J .C .M. Sterenborg, D. J. Robinson, and A. Amelink, "Method to quantitatively estimate wavelength-dependent scattering properties from multi-diameter single fiber reflectance spectra in a turbid medium," Opt. Lett. **36**, 2997–2999 (2011).
31. U. A.Gamm, S. C. Kanick, H .J .C .M. Sterenborg, D. J. Robinson, and A. Amelink, "Measurement of tissue scattering properties using multi-diameter single fiber reflectance spectroscopy: *in silico* sensitivity analysis," Biomed. Opt. Express **2**, 3150–3166 (2011).
32. U. A.Gamm, S. C. Kanick, H .J .C .M. Sterenborg, D. J. Robinson, and A. Amelink, "Quantification of the reduced scattering coefficient and phase-function-dependent parameter γ of turbid media using multidiameter single fiber reflectance spectroscopy: experimental validation," Opt. Lett. **36**, 1838–1840 (2012).
33. C. L. Hoy, U. A.Gamm, H .J .C .M. Sterenborg, D. J. Robinson, and A. Amelink, "Method for rapid multidiameter single fiber reflectance and fluorescence spectroscopy through a fiber bundle," J. Biomed. Opt. **18**, 107005 (2013).

1. Introduction

Fluorescence detection and quantification is important for many biomedical applications. For example, the detection of endogenous fluorophores such as NADH and FAD can indicate pathological alterations in tissues [1–3], while the quantification of exogenous compounds such as photosensitizers or chemotherapeutic agents that are fluorescent allows monitoring of drug distribution during photodynamic therapy (PDT) and chemotherapy [4–6].

In biomedical applications, the dependence of the detected fluorescence signal on the absorption and scattering properties of the tissue complicates its quantification. In order to quantitatively analyze fluorescence in tissue, it is important to obtain an intrinsic fluorescence signal that is independent of these optical property effects. Previously developed methods to extract intrinsic fluorescence spectra involve the acquisition of a paired measurement of fluorescence and white-light reflectance, where the latter is used to inform a correction of the influence of optical properties on fluorescence. This general approach has been extensively investigated for multi-fiber fluorescence probes, with separate source(s) and detectors [7–15]. These probes collect multiply scattered, or diffuse, light and sample volumes of tissue on the orders of several mm^3. An alternative approach for fluorescence measurements is to use small fiber optic probes that utilize a single optical fiber to both deliver excitation light and collect emitted fluorescence [16–20]; such a measurement results in a localized sampling volume, with the majority of the collected signal originating very close to the probe face [18].

Our group has recently published on the detailed mechanisms associated with the influence of scattering and absorption properties on the fluorescence intensity sampled by a single optical fiber [21, 22]. We showed, based on an extensive Monte Carlo simulated data set, that for a single fiber i) the measured fluorescence is proportional to the fiber diameter, and ii) the fluorescence as a function of scattering shows a bi-phasic effect where in the first phase fluorescence decreases with increased scattering and in the second phase fluorescence increases with increased scattering. In Fig. 1 Monte Carlo simulated data of single fiber fluorescence (SFF) intensity divided by the effective fiber diameter (F_{MC}^{sim}/d_{fib}) is plotted as a function of the product of the reduced scattering coefficient and the fiber diameter ($\mu_s' d_{fib}$). The observed bi-phasic effect was demonstrated to be the result of the combined effects of effective sampling volume, effective excitation fluence within the effective sampling volume and the collection probability of emitted photons from the effective sampling volume [21]. Furthermore, we showed that these combined effects can be mathematically described by an empirical model equation, cf. Eq. (5).

The aim of the current study is to develop an experimental SFF spectroscopy setup and validate the Monte Carlo data and semi-empirical model equation. To this end we will present a calibration procedure that corrects the SFF signal for all system-related, wavelength dependent transmission efficiencies to yield an absolute value of intrinsic fluorescence. We demonstrate the validity of the Monte Carlo data and semi-empirical model using a set of fluorescent

#203123 - $15.00 USD Received 17 Dec 2013; revised 9 Feb 2014; accepted 10 Feb 2014; published 22 May 2014
(C) 2014 OSA

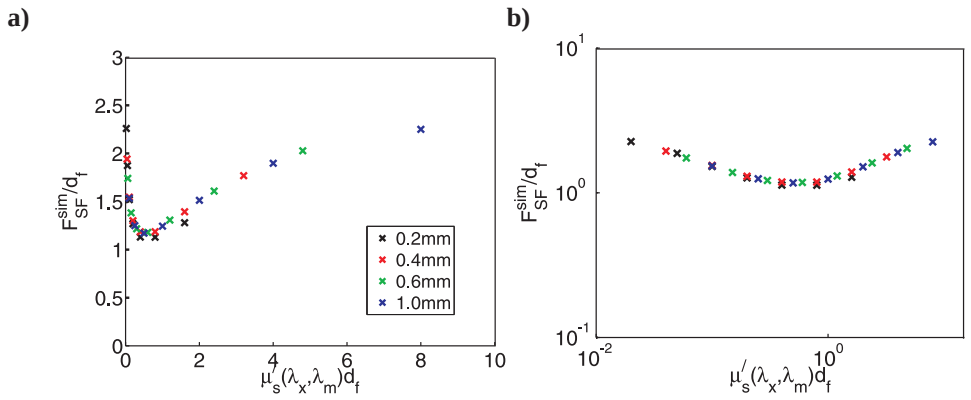

Fig. 1. Monte Carlo simulated data set of SFF intensity per fiber diameter, on (a) linear and (b) log scales.

phantoms with varying concentrations of Intralipid to vary the scattering properties, yielding a wide range of reduced scattering coefficients (μ_s' = 0-7 mm^{-1}). We also introduce a small modification to the model to account for the case of μ_s' = 0 mm^{-1} and show its relation to the experimental, simulated and analytically calculated value of SFF intensity in the absence of scattering. Finally, we demonstrate the accuracy of the method in the presence of absorption by performing measurements on phantoms which are fluorescing, scattering and absorbing.

2. Materials and methods

2.1. Theory

2.1.1. The SFF model

The intrinsic fluorescence ($F_i(\lambda_m)$ [nm^{-1} mm^{-1}]) is defined as the absolute fluorescence spectrum, independent of the optical properties of the medium, and is given by the product of the absorption coefficient of the fluorophore at the excitation wavelength ($\mu_a^f(\lambda_x)$) and the fluorescence quantum yield of the fluorophore ($Q^f(\lambda_m)$):

$$F_i(\lambda_m) = \mu_a^f(\lambda_x) Q^f(\lambda_m) \tag{1}$$

The total quantum yield Q^f is the integral of the wavelength dependent quantum yield $Q^f(\lambda_m)$:

$$Q^f = \int d\lambda_m Q^f(\lambda_m) \tag{2}$$

For the single fiber geometry, our group has recently investigated the influence of absorption and scattering properties on the collected fluorescence signal. We found, that the fluorescence signal can be corrected for absorption effects by using a modified Lambert-Beer law [22]:

$$F_{SF} = F_{SF}^0 e^{-\overline{\mu}_a \langle L_{SFF} \rangle} \tag{3}$$

Here, F_{SF}^0 is the corrected fluorescence signal, $\overline{\mu}_a$ is the average of the absorption coefficient at the excitation and emission wavelengths and $\langle L_{SF} \rangle$ is the average effective path length for SFF, which is given by:

$$\frac{\langle L_{SF} \rangle}{d_{fib}} = 0.71 \left(\overline{\mu}_s' d_{fib}\right)^{-0.36} \frac{1 + 1.81\sqrt{\overline{\mu}_s' d_{fib}}}{1 + \left(\overline{\mu_a} d_{fib}\right)} \tag{4}$$

#203123 - $15.00 USD Received 17 Dec 2013; revised 9 Feb 2014; accepted 10 Feb 2014; published 22 May 2014
(C) 2014 OSA

The effective path length is a function of the fiber diameter d_{fib}, $\overline{\mu}_a$ and $\overline{\mu}_s'$, the average scattering coefficient at the excitation and emission wavelengths.

The effect of scattering on the single fiber fluorescence signal leads to a bi-phasic behavior (Fig. 1), which our group has previously described by a semi-empirical model [21]:

$$\frac{F_{SF\ ratio}^{MC}(\lambda_m)}{\mu_a^f(\lambda_x)Q^f(\lambda_m)d_{fib}\nu_n} = 0.0935(\overline{\mu}_s' d_{fib})^{-0.31} e^{\left(\frac{-1}{0.31(\mu_s'(\lambda_x)d_{fib})+1} - \frac{1.61}{0.31(\mu_s'(\lambda_m)d_{fib})+1}\right)} \quad (5)$$

Here $F_{SF\ ratio}^{MC}$ is the ratio of the number of emission photons collected by the fiber and the number of excitation photons launched by the fiber, d_{fib} is the diameter of the single fiber probe and $\nu_n = \frac{1}{1+\varepsilon \cdot d_{fib}}$ is a parameter that accounts for the influence of the index of refraction mismatch at the fiber/medium and the annular air/medium interfaces (ε = 0.17 mm^{-1}). This ratio is a function of the reduced scattering coefficient μ_s' at the excitation wavelength (λ_x), emission wavelength (λ_m) and of the average reduced scattering coefficient at both wavelengths, $\overline{\mu}_s'$.

2.1.2. The case of μ_s'=0, μ_a=0

In the case of μ_s'=0 mm^{-1} and μ_a=0 mm^{-1}, fluorescence is unaltered by scattering and absorption and the total fluorescence intensity collected by the fiber (F_{SF}^0 [# photons]) depends on the fiber collection efficiency η, Q^f, $\mu_a^f(\lambda_x)$ and the excitation power (P_{laser} [# photons]), and is given by:

$$F_{SF}^0 = \int_0^\infty dz \eta Q^f \mu_a^f P_{laser} e^{-z\mu_a^f} = Q^f \mu_a^f P_{laser} \int_0^\infty dz \eta e^{-z\mu_a^f} \quad (6)$$

Here the fluorescence is implicitly integrated over all emission wavelengths and μ_a^f is at the laser excitation wavelength. The collection efficiency η for a fiber with diameter d_f and numerical aperture NA, for a fluorescent planar source with area A_s in a medium with refractive index n_0 is given by [23, 24]:

$$\eta = \frac{NA^2}{2n_0^2}\frac{\pi d_{fib}^2}{4A_s} \quad (7)$$

The area of the fluorescent source A_s is a function of distance from the fibertip z if the fiber itself is used to excite the fluorescence (see Fig. 2), i.e. $A_s = (\pi/4)d_{fib}^2(1+z/b)^2$, where b is the apparent point of origin of excitation light within the fiber:

$$b \approx \frac{d_{fib} n_0}{2NA} \quad (8)$$

Similar to the definition of $F_{SF\ ratio}^{MC}$, we define a fluorescence ratio $F_{SF\,ratio}^0$ [-] as the ratio of the number of fluorescent photons collected and the number of excitation photons launched for the zero-scattering case:

$$F_{SF\,ratio}^0 = \frac{F_{SF}^0}{P_{laser}} = Q^f \mu_a^f \int_0^\infty dz \eta e^{-z\mu_a^f} \quad (9)$$

Substitution of Eqs. (7) and (8) in Eq. (9), assuming the attenuation of the excitation light due to absorption by the fluorophores to be negligible (i.e. assuming μ_a^f is very small), and rearranging leads to

#203123 - $15.00 USD Received 17 Dec 2013; revised 9 Feb 2014; accepted 10 Feb 2014; published 22 May 2014
(C) 2014 OSA

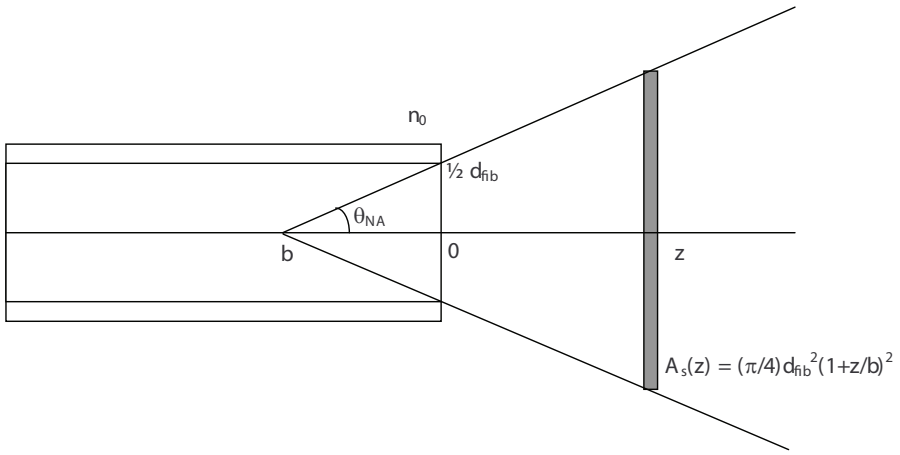

Fig. 2. Excitation and collection of fluorescence in a non-scattering medium using a single fiber.

$$\frac{F^0_{SF\,ratio}}{Q^f \mu_a^f} \approx \int_0^\infty dz \frac{NA^2}{2n_0^2} \left(\frac{1}{1+\frac{2NA}{d_{fib} n_0} z} \right)^2 = \frac{NA}{4n_0} d_{fib} \tag{10}$$

Thus the ratio $F^0_{SF\,ratio}/(Q^f \mu_a^f)$ is proportional to the fiber NA and the fiber diameter d_{fib} and equal to 0.041 for a fiber of $NA = 0.22$ and a medium of $n_0 = 1.33$. Based on this result the SFF-model Eq. (5) can be adapted to yield a value of 0.041 at μ_s'=0 mm^{-1}:

$$\frac{F^{MC}_{SF\,ratio}(\lambda_m)}{\mu_a^f(\lambda_x) Q^f(\lambda_m) d_{fib} v_n} = 0.0935(\bar{\mu_s'} d_{fib} + 0.00315)^{-0.31} e^{\left(\frac{-1}{0.31(\mu_s'(\lambda_x) d_{fib})+1} - \frac{1.61}{0.31(\mu_s'(\lambda_m) d_{fib})+1} \right)} \tag{11}$$

Note that in the transition from Eq. (10) to (11) we have reintroduced the v_n term to match the Monte Carlo results of our previous paper [21].

2.1.3. SFF calibration

The SFF-model was developed based on Monte Carlo simulations where the single fiber fluorescence signal was defined as the ratio of collected fluorescence photons (TMCP) and excitation photons launched (TXPL).

$$F^{MC}_{SF\,ratio} = \frac{TMCP}{TXPL} \tag{12}$$

Experimentally, we define the SFF ratio as

$$F^{exp}_{SF\,ratio}(\lambda_m) = \frac{F^{exp}_{SF}(\lambda_m)}{P_{laser}} \frac{\lambda_m}{\lambda_x} \tag{13}$$

Here $F^{exp}_{SF}(\lambda_m)$ [mW nm^{-1}] is the fluorescence collected by the single fiber and P_{laser} [mW] is the laser power at the distal end of the single fiber; the ratio of excitation and emission

#203123 - $15.00 USD Received 17 Dec 2013; revised 9 Feb 2014; accepted 10 Feb 2014; published 22 May 2014
(C) 2014 OSA

wavelengths corrects for the enery difference of photons at these different wavelengths. In an experimental setup, the total amount of **measured** fluorescent photons $F_{SF}^{meas}(\lambda_m)$ [counts s^{-1} nm^{-1}] is the product of the fluorescence collected by the single fiber, $F_{SF}^{exp}(\lambda_m)$, and the wavelength dependent transmission efficiency (including detector sensitivity) of the optical setup, $T_f(\lambda_m)$ [counts mJ^{-1}]:

$$F_{SF}^{meas}(\lambda_m) = F_{SF}^{exp}(\lambda_m)T_f(\lambda_m) \tag{14}$$

To retreive F_{SF}^{exp} from a measurement of F_{SF}^{meas}, we will determine T_f in a 2-step system calibration. First, a relative spectral calibration is performed by collecting a spectrum ($I_{cal}(\lambda)$) of a broadband calibrated light source of which the spectral output is known (in our case HL-2000-CAL, Ocean Optics, Duiven, Netherlands)).

$$I_{cal}(\lambda) = \alpha P_{cal}^{abs}(\lambda)T_f(\lambda) \tag{15}$$

Here $P_{cal}^{abs}(\lambda)$ [mW nm^{-1} cm^{-2}] is the absolute power spectrum of the calibrated light source as provided by the supplier and α [cm^2] is a wavelength-independent coupling factor that accounts for the fact that only a portion of the specified power from the calibrated lamp is coupled into the fiber. For the determination of α, which calibrates the system to an absolute intensity scale, a second calibration step is required.

In the second calibration step, a light source with a narrow bandwidth (e.g. laser or LED) is used. The wavelength of the light source is only of secondary importance; it should preferably be in a range of high system transmission efficiency to provide a good signal-to-noise ratio. In our case we have used an LED of 780 nm which is coupled into the system as shown in Fig. 3. Light from the LED is guided through the single fiber and exits the probe at its distal end. The wavelength-integrated power out of the fiber is measured with an integrating sphere (P_{LED}^{meas} [mW]) and a reflectance spectrum is recorded by submerging the probe tip into a calibration phantom with a known reflectance ($R_{IL}(\lambda)$ [-]). Here we use a phantom that contains Intralipid as scatterer with a $\mu_s'(600nm)$= 1.8 mm^{-1} [25]. Its absolute single fiber reflectance $R_{IL}(\lambda)$ for all used fiber diameters was previously determined through Monte Carlo simulations.

The collected spectrum $I_{LED}(\lambda)$ [counts s^{-1} nm^{-1}] is given by:

$$I_{LED}(\lambda) = P_{LED}^{abs}(\lambda)T_f(\lambda)R_{IL}(\lambda) \tag{16}$$

Since we do not measure the LED power spectrum but its total power output, Eq. (16) has to be integrated over wavelength:

$$P_{LED}^{meas} = \int P_{LED}^{abs}(\lambda)d\lambda = \int \frac{I_{LED}(\lambda)}{T_f(\lambda)R_{IL}(\lambda)}d\lambda \tag{17}$$

Eqs. (13) - (17) can be combined to yield $F_{SF\ ratio}^{exp}(\lambda_m)$:

$$F_{SF\ ratio}^{exp}(\lambda_m) = F_{meas}^{SF}(\lambda_m)\frac{\lambda_m}{\lambda_x}\frac{P_{LED}^{meas}}{P_{laser}}\frac{P_{cal}^{abs}(\lambda)}{I_{cal}(\lambda)}\int \frac{I_{cal}(\lambda)R_{IL}(\lambda)}{I_{LED}(\lambda)P_{cal}^{abs}(\lambda)}d\lambda \tag{18}$$

2.2. Experimental methods

2.2.1. Single fiber fluorescence setup

A schematic diagram of the single fiber fluorescence setup is shown in Fig. 3. It consists of a spectrometer (QE-4000, Ocean Optics, Duiven, The Netherlands), a 405 nm diode laser (PPMT-45(405-60), Power Technology, Little Rock, USA) for excitation, a 780 nm LED for calibration and a solid core multi-mode fiber which is connected to the other components through a

#203123 - $15.00 USD Received 17 Dec 2013; revised 9 Feb 2014; accepted 10 Feb 2014; published 22 May 2014
(C) 2014 OSA

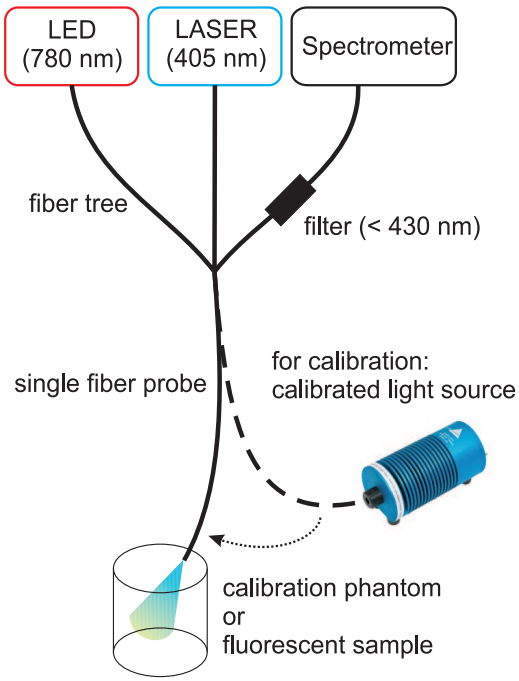

Fig. 3. Schematic diagram of the experimental SFF setup.

trifurcated optical fiber. During measurements, excitation light is emitted from the laser and travels to the distal end of the single fiber from where it enters the medium. Inside the medium fluorescence is generated and a fraction of it reenters the single fiber and is detected by the spectrometer. Reflected excitation light is filtered out by a 430 nm high pass filter in front of the spectrometer.

2.2.2. Fluorescent phantom measurements

We prepared scattering phantoms by mixing different concentrations of Intralipid 20% (Fresenius Kabi, s-Hertogenbosch, Netherlands) with PBS (J.T.Baker, Deventer, Netherlands), with resulting reduced scattering coefficients of $\mu_s'(405nm)$=[0, 0.005, 0.01, 0.05, 0.11, 0.16, 0.22, 0.33, 0.55, 0.83, 1.1, 2.19, 3.3, 4.38, 5.46, 6.58] mm^{-1} [25]. To add fluorescence to the phantoms, fluorescein (Sigma Aldrich, Zwijndrecht, The Netherlands) was dissolved in PBS and mixed into the phantoms, yielding a final concentration of 1 μM. The absorption coefficient μ_a^f of fluorescein was measured in a spectrophotometer (UV2101PC, Shimadzu,'s-Hertogenbosch, The Netherlands) and determined to be $\mu_a^f(405\text{ nm}) = 5.75 \cdot 10^{-5}\ mm^{-1}$ for a 1 μM solution.

To show that the SFF signal can be corrected for absorption, we prepared phantoms with 1 μM fluorescein dissolved in PBS, Intralipid ($\mu_s'(405nm)$=0.83 mm^{-1}) and added isolated red blood cells (RBCs) as absorber. The RBCs were isolated from the plasma by three cycles of centrrifugation (7 min, 2000 rpm, 21 degrees) and subsequent resuspension of the RBC pellet in PBS. Four phantoms were prepared with 0, 0.25, 0.5 and 1 % of RBCs, which led to absorption coefficient of $\overline{\mu_a}$ = [0, 0.64, 1.3, 2.6] mm^{-1}. Absorption coefficients were determined from single fiber reflectance (SFR) measurements [27]. One last phantom was prepared with Intralipid ($\mu_s'(405nm)$=0.83 mm^{-1}), RBCs ($\overline{\mu_a}$ = 0.68 mm^{-1}) and 1μM fluorescein which was incubated in 2 M of BSA for half an hour prior to mixing with RBCs and Intralipid to avoid binding of

#203123 - $15.00 USD Received 17 Dec 2013; revised 9 Feb 2014; accepted 10 Feb 2014; published 22 May 2014
(C) 2014 OSA

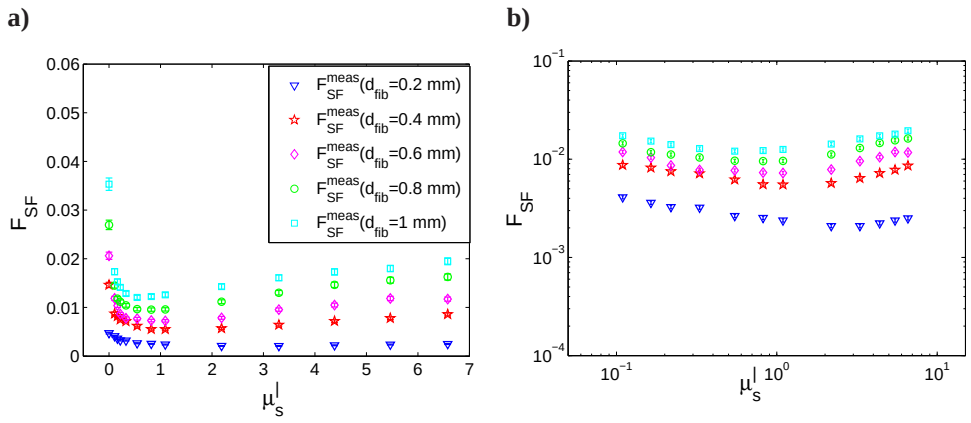

Fig. 4. Integrated $F^{exp}_{SF\ ratio}$ signals (abbreviated as F_{SF}) of 5 different fiber diameters vs. reduced scattering coefficient (μ_s') in linear (a) and logarithmic scale (b).

the fluorescein with the RBCs. Combined SFF and SFR measurements were performed with a single fiber probe with the diameter d_{fib}=0.6 mm.

It has been shown that the dianionic state of fluorescein is predominantly present in a solution with a pH of 7.4 [26]. The fluorescence quantum yields of the dianion and the anion are 0.93 and 0.37, respectively, and with a 90% contribution of the dianion, the fluorescence quantum yield of our phantoms was therefore estimated to be Q^f = 0.87.

SFF measurements were performed superficially with 5 different fiber diameters (d_{fib}=[0.2, 0.4, 0.6, 0.8, 1] mm) by bringing the bare fiber probe just in contact with the liquid phantom. This was done by continuously monitoring white light emerging from the fiber tip and slowly bringing the phantom surface closer to the fiber using a labjack; a noticeable change in the white light output profile was visible as soon as the tip touched the liquid surface due to the change in medium refractive index. To correct for background signals and fluorescence caused by Intralipid itself, spectra of phantoms with the same Intralipid concentrations but without fluorescein were taken as well and subtracted from the spectra of the scattering and fluorescent phantoms. The system was calibrated as described above (Eq. (18)) and the resulting $F^{exp}_{SF\ ratio}(\lambda_m)$spectra were integrated over the emission wavelength. For comparison of the data with the semi-empirical model (Eq. (11)), the integrated $F^{exp}_{SF\ ratio}$ signal was divided by $\mu_a^f Q^f d_{fib} \nu$.

3. Results

3.1. SFF measurements on scattering phantoms

Fig. 4 shows the integrated $F^{exp}_{SF\ ratio}$ of five different fiber diameters versus μ_s' on linear and log scales. As mentioned previously, the bi-phasic behavior of the curves is caused by the combined effect of a decrease in sampling volume and an increase in excitation fluence and collection probability with increasing scattering. When the fluorescence is divided by its corresponding fiber diameter, as shown in Fig. 5, all five curves nearly collapse onto each other and when plotted as a function of dimensionless reduced scattering ($\mu_s' d_{fib}$) the curve follows the Monte Carlo simulated data (black dots in Fig. 5) as well as the SFF model (blue line) quite well, proving the validity of the model and the experimental calibration procedure.

#203123 - $15.00 USD Received 17 Dec 2013; revised 9 Feb 2014; accepted 10 Feb 2014; published 22 May 2014
(C) 2014 OSA

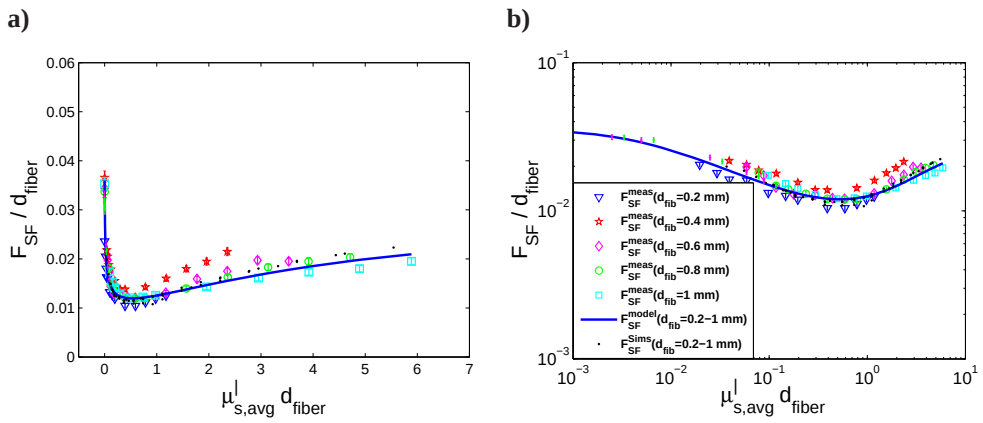

Fig. 5. SFF signal per fiber diameter vs. dimensionless reduced scattering ($\mu_s' d_{fib}$) in linear (a) and logarithmic scale (b). Black dots denote Monte Carlo simulated data for all fiber diameters and blue line is the adapted SFF model (Eq. (11)).

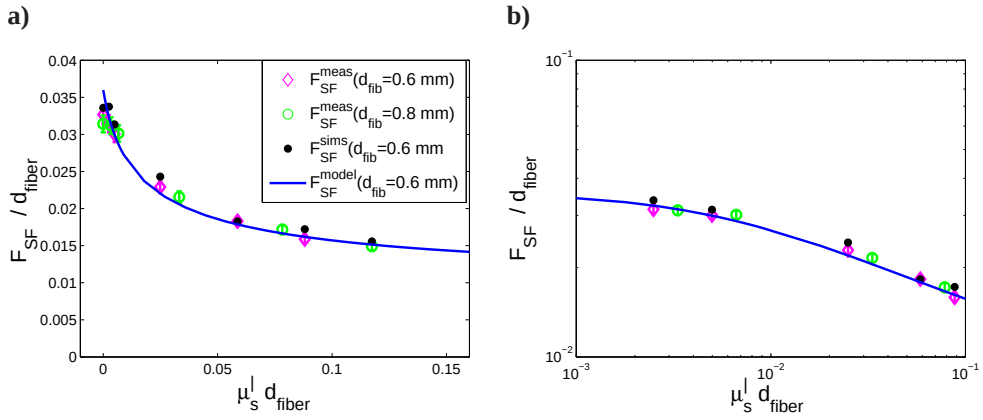

Fig. 6. SFF signal per fiber diameter vs. dimensionless reduced scattering ($\mu_s' d_{fib}$) for low scattering (μ_s' =0 - 0.22 mm^{-1}) and for two fiber diameters (d_{fib}=0.6, 0.8 mm). Black dots denote Monte Carlo simulated data for d_{fib}=0.6 mm and the blue line is the adapted SFF model (Eq. (11)). Linear (a) and logarithmic scales (b).

#203123 - $15.00 USD Received 17 Dec 2013; revised 9 Feb 2014; accepted 10 Feb 2014; published 22 May 2014
(C) 2014 OSA

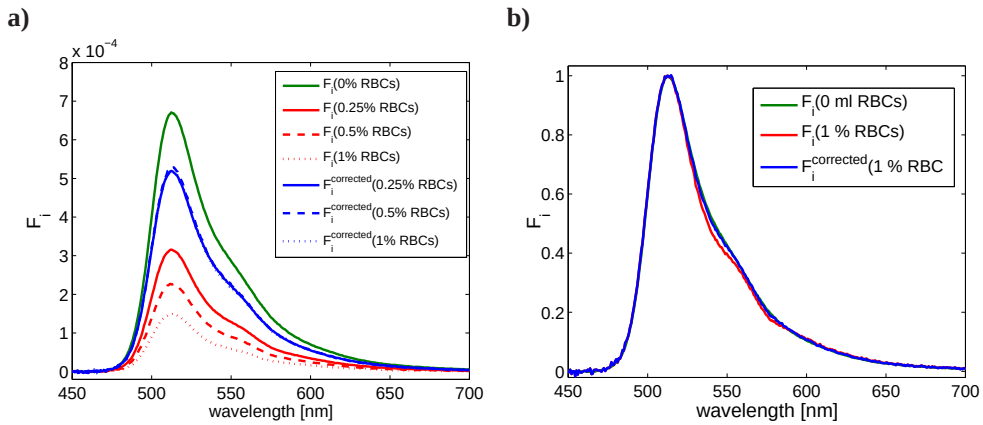

Fig. 7. Measured intrinsic Fluorescence in presence of scattering (Intralipid: μ_s' = 0.82 mm^{-1}) and absorption (RBCs: c=[0, 0.25, 0.5, 1]% , $\overline{\mu_a}$ = [0, 0.64, 1.3, 2.6] mm^{-1}) a) Fluorescence signal F_i of non-absorbing phantom (green line), uncorrected Fluorescence signal F_i (red lines) and corrected Fluorescence signal F_i (blue lines) of absorbing phantoms. b) Normalized fluorescence spectra show how the shape of the uncorrected (red line) fluorescence spectrum is distorted by the presence of blood in comparison to the spectrum of the non-absorbing (green line) phantom and the corrected spectrum (blue line).

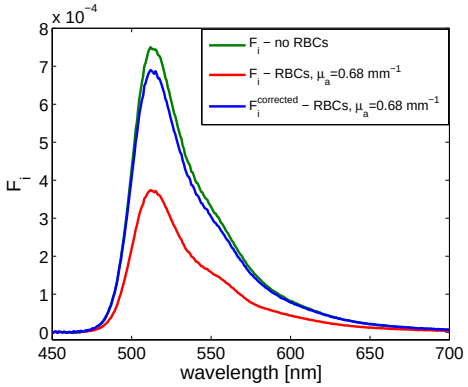

Fig. 8. In order to avoid binding of fluorescein with the RBCs, fluorescein ($1\mu M$) was incubated with 2M BSA for 30 min before mixing with RBCs ($\overline{\mu_a}$ = 0.68 mm^{-1}) and Intralipid (μ_s' = 0.82 mm^{-1}). Differences between spectra of the non-absorbing phantom (green line) and the corrected absorbing phantom (blue line) are 7%.

#203123 - $15.00 USD Received 17 Dec 2013; revised 9 Feb 2014; accepted 10 Feb 2014; published 22 May 2014
(C) 2014 OSA

3.2. SFF measurements in the very low scattering regime

The SFF model was adapted to be valid in the case of $\mu_s' = 0\ mm^{-1}$ based on an analytical derivation. A very good correlation between the model, simulations and experimental SFF measurements of low scattering phantoms is demonstrated in Fig. 6.

In the case of $\mu_s' = 0\ mm^{-1}$ the calculated value of the collected fluorescence is not accounting for absorption of excitation light within the medium and assumed collection of photons up to infinity, which leads to a slight overestimation of collected fluorescence compared to our phantoms where $\mu_a^f(405\text{ nm}) = 5.75 \cdot 10^{-5}\ mm^{-1}$ and the distance from probe tip to the bottom of the container is roughly 15 mm. Numerical evaluation of Eq. (10) for this μ_a^f value yields $F_{SF\ ratio}^{exp}/\mu_a^f Q^f d_{fib} \nu \approx 0.037$ for an integration depth up to 15 mm. The experimental value (average of 5 fiber diameters) was 0.033 ± 0.005 which is in agreement with the analytical value for the zero scattering case.

3.3. SFF measurements on scattering and absorbing phantoms

In order to demonstrate the validity of the absorption-correction which we presented in the theory part (Eq.3 and 4), we created phantoms which contained fluorescein, Intralipid as scatterer and isolated red blood cells ($\overline{\mu_a}$ = 0.6, 1.3, 2.6 mm^{-1}) as absorbers. Fig. 7 a) displays how the fluorescence spectra of phantoms with different amounts of RBCs (red lines) are attenuated in comparison to the non-absorbing phantom which contains only fluorescein and Intralipid. When the three spectra with different amounts of RBCs are corrected for the effect of absorption, they collapse onto the same curve (blue lines in Fig. 7a). The spectral shapes of the corrected spectra are identical to the shape of the undistorted spectrum (Fig. 7b), but the amplitude of the corrected spectra is 15% smaller than of the undistorted spectrum. Since it is known that fluorescein tends to bind to RBCs [29], we hypothesize that this is the case in our phantom and that through the binding process the fluorescence is being quenched.Therefore we created one additional phantom with Intralipid as scatter and RBCs as absorber, but incubated the fluorescein in a 2M solution of BSA prior to adding the RBCs and Intralipid [28]. In this way, fluorescein would bind to BSA, which does not quench the fluorescence and prevents that fluorescein binds to the RBCs. The result of this experiment is shown in Fig. 8. In this case, the difference between the corrected and undistorted spectrum is reduced to 7%.

4. Discussion and conclusion

We have developed a single fiber based spectroscopic method, that allows a full quantification of the intrinsic fluorescence in a turbid medium. We have shown, using an extensive set of phantoms, that the collected single fiber fluorescence indeed shows a bi-phasic behavior with increasing scattering, and proved the validity of the semi-empirical SFF model which was published previously (Eq. (5)).

Furthermore, we have presented a calibration procedure that corrects for system transmission properties, enabling measurement of the intrinsic fluorescence ($\mu_a^f Q^f$) in a turbid medium. Note that calculation of the intrinsic fluorescence from the measured calibrated fluorescence requires knowledge of the reduced scattering coefficient of the medium at excitation and emission wavelengths; in case of phantoms such as used in this study these properties are well known. Moreover, we recently published a series of papers on the development of multi-diameter single fiber reflectance spectroscopy (MDSFR) which allows the determination of the reduced scattering coefficient of a turbid medium by measuring white-light reflectance spectra with multiple fiber diameters [30–32]. MDSFR and SFF can be easily combined in the same setup to perform subsequent white-light reflectance and fluorescence measurements [33], which allows the quantification of the intrinsic fluorescence even in media where the reduced scattering coef-

#203123 - $15.00 USD Received 17 Dec 2013; revised 9 Feb 2014; accepted 10 Feb 2014; published 22 May 2014
(C) 2014 OSA

ficient is not known *a priori*. Additionally, the MDSFR measurement does not only yield μ_s' but also allows quantification of the absorption coefficient μ_a of endogenous and exogenous tissue absorbers, including μ_a^f of the fluorophore itself if it is sufficiently high. Independent measurement of μ_a^f through MDSFR allows, when combined with an SFF measurement of $\mu_a^f Q^f$, the determination of the fluorescence quantum yield Q^f *in vivo*, which, to the best of the authors knowledge, is not possible with other optical methods. Knowledge of the quantum yield *in vivo* could play an important role in the design of new photosensitizers that could be customized for specific tissues. Furthermore, if the pH dependence of the quantum yield of a specific fluorophore is known, which is the case for e.g. fluorescein, the combined SFF/MDSFR method could be used for *in vivo* pH sensing [26]. Note that the fiber-bundle setup for MDSFR measurements [33] also easily facilitates reflectance measurements at a source-detector separation of 0.5 mm. The effective path-lengths of these photons are much longer than of the photons that contribute to the MDSFR signal, thereby increasing the sensitivity to absorption and allowing much smaller μ_a^f values to be measured compared to MDSFR alone.

The SFF model was successfully modified to meet the requirements for SFF measurements in a medium that contains little or no scattering. A small discrepancy was observed between the analytical and experimental fluorescence values at zero scattering; this is most likely related to the assumptions made in the analytical calculation, i.e. no attenuation of the excitation beam and collection of photons up to infinity. Both these assumptions are not met in the experimental situation, leading to a smaller experimental value compared to the analytical solution. Another small discrepancy between experimental data and Monte Carlo data is observed in the scattering case; while for the MC data the fluorescence scales perfectly with fiber diameter, some fiber-diameter dependent variations are observed experimentally (Fig. 5). These variations do not show a systematic trend, i.e. the 200 micron data are slightly lower while the 400 micron data are slightly higher than the fluorescence of the other fiber diameters, for all scattering coefficients. These deviations most likely originate from the experimental calibration procedure. Potential errors introduced in that step might be related to the assumption that α is wavelength independent to the Monte Carlo simulated reflectance R_{IL} and to the power measurements of the calibration LED and the laser (P_{LED}^{meas} and P_{laser}). Finally, it should be noted that the MC simulations and thus the SFF model were designed for superficial measurements. Therefore, experimental measurements were also performed superficially. We did observe that the SFF signal is different in interstitial measurements, depending on scattering, fiber diameter and measurement depth; the behavior of the SFF signal in interstitial situations is a topic of future investigation.

We demonstrated that fluorescence measurements in presence of absorption can be corrected by applying a modified Lambert-Beer law. We have shown that the correction method worked for fluorescence measurements on phantoms containing Intralipid as scatterer and different concentrations of isolated red blood cells as absorbers. The fact, that the corrected fluorescence signal did not reach the height of the signal acquired from a non-absorbing phantom is likely to be caused by a quenching effect that occurs when fluorescein binds to RBCs. In order to test this hypothesis, we bound fluorescein to BSA before adding the RBCs and found that the corrected signal almost reached the signal of the phantom without absorber. The small difference between the amplitudes of the absorption-corrected and undistorted spectra of 7% may be caused by a smaller fraction of fluorescein molecules that were not bound or dissociated from their bond with BSA and were subsequently quenched through binding to the RBCs.

In conclusion, we have developed a fiber-optic method that allows the quantification of the intrinsic fluorescence in a turbid medium using a single optical fiber. We have demonstrated the feasibility of the method and the validity of the SFF model through measurements on a wide range of scattering and fluorescent phantoms.

#203123 - $15.00 USD Received 17 Dec 2013; revised 9 Feb 2014; accepted 10 Feb 2014; published 22 May 2014
(C) 2014 OSA